Nanoscale Advances

ROYAL SOCIETY OF CHEMISTRY

PAPER

View Article Online
View Journal | View Issue

Cite this: *Nanoscale Adv.*, 2021, **3**, 2862

Experimental measurement of local high temperature at the surface of gold nanorods using doped $ZnGa_2O_4$ as a nanothermometer†

Estelle Glais, [ab] Agnès Maître, [c] Bruno Viana [b] and Corinne Chanéac *[a]

Heat measurement induced by photoexcitation of a plasmonic metal nanoparticle assembly under environmental conditions is of primary importance for the further development of applications in the fields of (photo)catalysis, nanoelectronics and nanomedicine. Nevertheless, the fine control of the rise in temperature remains difficult and limits the use of this technology due to the lack of local temperature measurement tools working under environmental conditions. Luminescence nanothermometers are an alternative solution to the limitations of conventional contact thermometers since they are able to give an absolute temperature value with high spatial resolution using common optical equipment. As a proof of concept of this nanothermometry approach, a high local temperature exceeding one hundred degrees is measured on the thermalized photoexcited aggregate of gold nanorods using $ZnGa_2O_4:Cr^{3+},Bi^{3+}$ nanothermometers that have a strong temperature dependence on the luminescence lifetime of chromium(III) and high sensitivity over an extensive range of temperatures. A study on the influence of the average distance between nanosensors and nanoheaters on the measured temperature is carried out by coating the nanosensors with a silica layer of tunable thickness, highlighting the temperature gradient at the vicinity of the nanoheater as the theory predicts. The variation of the optical nanosensor response is relevant and promising, and it could be further envisioned as a potential candidate for local temperature measurement at the nanoscale since no plasmonic effect on Cr^{3+} lifetime is observed. The results reported here open up an even wider field of application for high temperature nanothermometry on real samples such as aggregate particles for many applications including catalysis and nanoelectronics. Thermometry using luminescent nanoprobes, which is complementary to thermal microscopy techniques, will allow *in situ* and *in operando* temperature monitoring at very small scales.

Received 4th January 2021
Accepted 23rd March 2021

DOI: 10.1039/d1na00010a

rsc.li/nanoscale-advances

Introduction

Precise temperature measurement at the nanoscale is a very challenging topic of interest and has attracted numerous investigations over the past decade. Indeed, it will offer many new possibilities in medicine like early detection of illnesses and improvements of diagnosis, since one of the first signature of a disease is the existence of thermal irregularities.[1,2] Such non-invasive temperature measurements are also needed during hyperthermia therapies in order to optimize and control the temperature increase at the sub-cellular scale,[3] and limit the diseases of tissues. Furthermore, due to the miniaturization of electronics, a nanoscale, contactless and nondestructive measurement of the temperature will also be a real asset for early hotspot detection, leading to a lifetime increase for such devices. In the field of catalysis assisted by magnetic or plasmonic induction, a thermal nanosensor will be a valuable tool for understanding mechanisms as well as highlighting heat transfer and heat dissipation.[4] One can see the importance of developing new tools for local measurement of temperature based on photoacoustic[5] imaging or luminescence emission.[6] Recently, several luminescent nanosensors have been developed in this respect.[7–11] Thanks to their thermal dependent optical properties, they allow a self-referenced, accurate and contactless temperature determination. Interestingly, gold nanoparticles can be used both as a nanothermometer and nanoheater.[12] Gold nanoparticles are well known for their ability to generate heat after optical excitation. Indeed, under an appropriate excitation wavelength, collective motion of surface electrons is induced, called surface plasmon resonance (SPR). This phenomenon is responsible for the temperature increase

[a]*Sorbonne Université, CNRS, Collège de France, UMR 7574, Laboratoire de Chimie de la Matière Condensée de Paris, 4 Place Jussieu, 75005 Paris, France. E-mail: corinne.chaneac@sorbonne-universite.fr*

[b]*PSL Research University, IRCP, Chimie ParisTech, CNRS, 11 rue P. et M. Curie, 75231 Paris Cedex 05, France*

[c]*Sorbonne Université, CNRS, UMR 7588, Institut des Nanosciences de Paris, 4 Place Jussieu, 75005 Paris, France*

† Electronic supplementary information (ESI) available. See DOI: 10.1039/d1na00010a

of the particle and of its surroundings.[13–15] Light-to-heat conversion quantification has attracted numerous theoretical investigations. Gold nanoparticles also exhibit a stable luminescence due to the enhancement of the cross-section at the SPR despite a low quantum yield (around 10^{-6}). Combining both properties, when they are thermalized using pulse-laser irradiation, local temperature can be deduced from the spectrum of the anti-Stokes emission without the need for any previous calibration.[16] Nevertheless, this method, although very attractive, requires working on single particles and with thermal microscopy techniques which means that temperature monitoring *in situ* and with aggregate particles is not possible, as in most current cases. In addition, temperature accuracy of gold nanoparticles is quite low (4 K). Another approach is to consider separated nanoheaters and nanothermometer functions.[17–23] Experimental methods have recently been developed, as a result of the emergence of new temperature nanoprobes. Rocha *et al.*[17] have investigated core/shell LaF_3:Nd^{3+}/LaF_3 nanoparticles coupled with gold nanorods (GNRs). Looking at the relative intensity ratio of Nd^{3+} emission, they highlighted the possibility of a sub-tissue thermal sensing and demonstrated the suitability of such combined systems for photothermal therapy application. Maestro *et al.*'s[18,20] investigations focused on the spectral shift of the CdSe Quantum Dot (QD) emission band and successfully internalized both CdSe QDs and GNRs in a cell, showing the temperature increase inside a HeLa cell. Nigoghossian *et al.*[22] and Huang *et al.*[23] have studied $NaGdF_4$:Er^{3+},Yb^{3+} up-converting nanoparticles (UCNPs) as a thermal sensor with a fixed distance between nanoheaters and nanothermometers by developing new core/shell nanoheater/UCNP heterostructures. All these pioneering studies focused on nanothermometers (UCNPs and QDs) that are able to detect temperature variation in a restricted temperature range (from 20 to 70 °C), which is suitable for biological applications. In this work, we propose to study a combined nanothermometer/GNR system, allowing enlargement of the probed temperature range, which is up to now an unexplored area and could be a real key asset especially in the field of catalysis or nanoelectronic devices.

In our previous work,[24] we demonstrated the abilities of zinc gallate oxide nanoparticles doped with chromium(III) and bismuth(III): $ZnGa_2O_4$:$Cr^{3+}_{0.5\%}$,$Bi^{3+}_{0.5\%}$@SiO_2 as nanothermometers (ZGO-NThs). These ZGO-NThs, less than 10 nm in diameter, present very good properties in the 20 to 200 °C temperature range with a maximal relative sensitivity of 1.9% $°C^{-1}$. Indeed, the Cr^{3+} emission centered at 700 nm originates from the contribution of two trivalent chromium transitions: $^2E \rightarrow {}^4A_2$ and $^4T_2 \rightarrow {}^4A_2$.[25–27] Since the ^2E and $^4T_2$ levels are in thermal equilibrium, the temperature increase leads to an increase of the $^4T_2 \rightarrow {}^4A_2$ spin allowed transition at the expense of the $^2E \rightarrow {}^4A_2$ spin forbidden transition.[28] Thus, between 20 °C and 200 °C, the Cr^{3+} lifetime value drastically decreases when the temperature increases. The lifetime value is a relevant parameter for temperature quantification, since it allows an absolute and self-referenced temperature measurement. In addition, the thermal and chemical stabilities of the ZGO-NTh have been highlighted making these nanophosphors very robust and reliable thermal sensors.[24]

The aim of our article is to propose alternative measurement methods namely nanothermometry with luminescent nanoparticles that are more local than infrared probe measurements and that can be carried out in environments as complex as measurement on a small animal or inside a heterogeneous catalysis reactor for example. For that, the optical devices used are common and adapted for contact measurements at the nanometer scale on real samples (particle aggregates, supported particles, …). Measurements of heat elevation of GNRs induced by continuous optical excitation are taken using a luminescent nanothermometer to highlight the possibility of a local temperature measurement over a wide range. First, we compare the ZGO-NTh response coupled to GNR nanoparticles under irradiation, then we present the influence of the average distance between the nanothermometer and the nanoheater on the measured temperature by varying the thickness of the silica layer around the ZGO-NTh. Indeed, the measured local temperatures in the vicinity of the gold nanoheater are much higher than the ones observed by NIR thermal camera, showing the ability of the ZGO-NTh to probe the average temperature at the nanoscale in a scarcely explored temperature range.

Results and discussion

The performance of the ZGO-NTh has already been reported in a previous study,[24] but for further clarity, the XRD pattern and the calibration curve are presented in Fig. SI-1 and 2,† respectively. The experimental lifetime τ_{exp}, determined from the decay curve following eqn (1), presents a huge decrease with temperature increase.

$$\tau_{exp} = \frac{\int I(t) t \mathrm{d}t}{\int I(t) \mathrm{d}t} \quad (1)$$

This variation is attributed to thermal activation of the spin allowed $^4T_2 \rightarrow {}^4A_2$ characterized by shorter lifetime values in regard to the spin forbidden $^2E \rightarrow {}^4A_2$ transition (see SI-3†). At low temperature, the emission is mainly due to the $^2E \rightarrow {}^4A_2$ transition. It is possible to adjust this phenomenon according to the following equation, adapted from Labeau *et al.*,[29] which models a thermal equilibrium between two levels involved in the radiative deexcitation processes:

$$\tau_{fit}(T) = \frac{1 + \exp(-\Delta E/k_B T)}{\Gamma_F + \Gamma_A \exp(-\Delta E/k_B T)} \quad (2)$$

where ΔE corresponds to the energy difference between ^2E and $^4T_2$, k_B is the Boltzmann constant and Γ_A and Γ_F are the radiative channels corresponding to the $^4T_2 \rightarrow {}^4A_2$ and $^2E \rightarrow {}^4A_2$ transitions, respectively. The fitting curve is presented as a dashed line in Fig. SI-2.† For our system, the obtained ΔE value is about 2643 ± 48 cm^{-1}, which is smaller than calculated values on bulk materials already reported in the literature

(3814 cm^{-1} (ref. 18) and 3754 cm^{-1} (ref. 30)), as well as for $MgTiO_3:Mn^{4+}$ nanoparticles.[31]

Once the calibration is effective, ZGO-NThs are coupled to the nanoheater in order to measure a local temperature increase. Gold nanorods have been chosen as a nanoheater owing to their spectral features (Fig. 1a). The localized surface plasmon resonance observed in metallic small size particles results in absorption in the visible range. For spheres, the absorption band is located at around 520 nm (Fig SI-4b† inset, light red curve). In the case of nanorods, the polarization of light allows the excitation of several plasmons. As the plasmon resonance shifts in the red as the aspect ratio increases, two absorption bands are observed: one band in the infrared range corresponding to the polarization according to the large dimension of the object induced by a collective oscillation of the electrons in this direction and a second one in the green corresponding to the wave polarized in the transverse direction (Fig. 1a, black curve). Indeed, ZGO-NThs present an emission (red curve) centered at 700 nm under 430 nm pulsed laser excitation. In order to (i) avoid the parasitic excitation of GNRs during the measurement and (ii) avoid the reabsorption of ZGO-NTh emission by GNRs, an aspect ratio of 6 was chosen for nanorods. Thus 60.4 ± 10.6 nm by 9.0 ± 1.4 nm GNRs were synthesized (Fig. 1b). At this size, the longitudinal plasmon band is centered at 1060 nm with a typical width of 300 nm, allowing 976 nm plasmon excitation (Fig. 1a) without any disturbance of the nanothermometer.

The temperature increase induced by photoexcitation of GNRs at 976 nm in aqueous solution is first demonstrated and compared to a control sample of spherical nanoparticles that do not absorb at this wavelength (Fig. SI-4†). The nanoparticles with various shapes (spheres and rods) in aqueous suspensions are irradiated under the same conditions and the temperature is followed using a NIR thermal camera. In both cases, after 10 minutes of 976 nm laser diode irradiation (3 W cm^{-2}), the temperature reaches a plateau, which is higher in the case of gold nanorods than in the gold nanosphere suspension ($\Delta T = 6$ °C). The observed transient regime corresponds to medium thermalization. In the nanosphere solution, as such gold nanoparticles do not absorb at this wavelength, the temperature increase, due to the power of the laser, remains low. An increase of the temperature is observed for nanorods compared to nanospheres, highlighting the strong absorption efficiency and light to heat conversion of the synthesized GNRs when exciting in the plasmon band. Thus both nanoheaters and nanothermometers (1 : 10) are introduced in the same medium in order to quantify precisely the temperature increase at the nanometric scale due to the plasmon effect.

Fig. 2a shows a TEM picture of the studied samples (ZGO-NThs/GNRs). Both ZGO-NThs (spheres 11.4 nm in diameter) and GNRs are clearly identifiable here as well as in the cryo-TEM pictures presented in Fig. SI-5.† The experimental setup is presented in Fig. 2b. The sample is simultaneously irradiated by a pulsed laser ($\lambda = 430$ nm, 10 Hz, nanothermometer excitation) and by a continuous laser diode (λ = 976 nm, nanoheater irradiation). The temperature is followed by a thermal camera, and luminescence lifetime is recorded through a photomultiplier coupled to an oscilloscope. It is important to notice that for luminescence lifetime measurements, the ZGO-NTh/GNR sample under only 430 nm irradiation could be considered as a reference in order to overcome any disturbance in nanothermometer optical properties due to the presence of the GNR. Indeed, no variation of the decay profile is observed upon the addition of gold nanoparticles thus permitting the experience to be validated (Fig. SI-6†). It suggests that no quenching phenomenon induced by the GNR occurs at such distance. In the last part, the influence of the distance between the ZGO-NTh and GNR is investigated.

Luminescence decay of the ZGO-NTh/GNR sample after 30 min irradiation with a 976 nm laser diode is presented in Fig. 2c (red curve). The exponential profile is comparable to the reference sample (in grey); only the slope strongly varies revealing the large temperature variation under 976 nm excitation. Thus temperatures can be determined using the temperature calibration curve presented in Fig. SI-1.† Fig. 2e presents the variation of temperature measured by the NIR thermal camera according to the laser diode excitation time. After 30 minutes under laser diode excitation, the temperature of the ZGO-NTh/GNR sample reaches 48 °C while the suspension of the ZGO-NTh alone reaches only 38 °C. In Fig. 2d the ZGO-NTh lifetime is plotted *versus* laser diode excitation time. The deduced temperature is higher (60 ± 3 °C) than the one

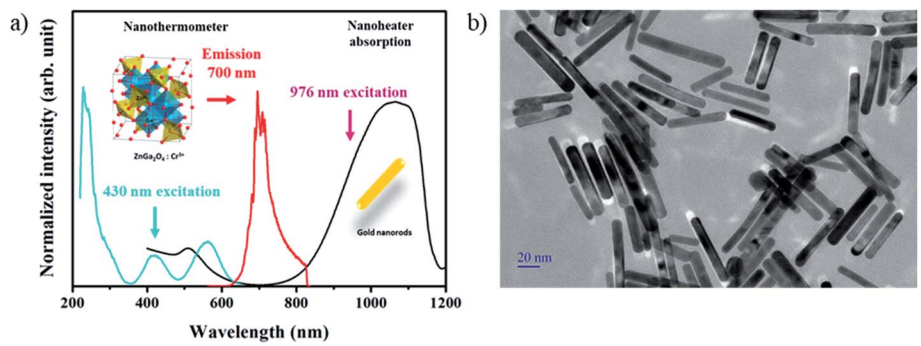

Fig. 1 (a) Excitation (blue) and emission (red) spectra of the ZGO nanothermometer, and absorption spectrum of the GNR nanoheater, and (b) TEM picture of GNRs.

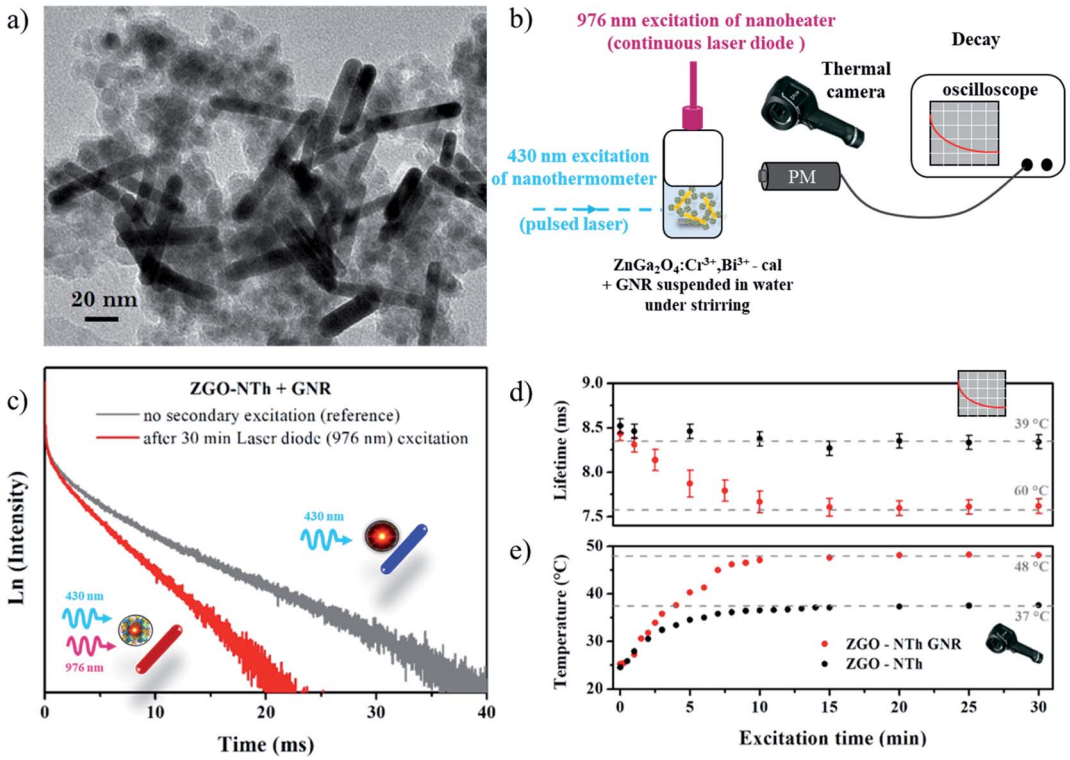

Fig. 2 (a) TEM picture of the studied sample. (b) Schematic representation of the experimental setup used for the temperature determination. (c) Decay profiles of the ZGO-NTh/GNR sample with (red) and without (grey) laser diode excitation (976 nm). (d) Temperature variation according to the laser diode excitation time measured by luminescence lifetimes of the nanosensor and (e) measured by an NIR thermal camera.

obtained using thermal camera pictures (48 °C ± 2 °C). These results highlight that while the thermal camera picture gives a global temperature on the reactor surface characteristic of water thermalization, the ZGO-NTh allows a local average temperature measurement in the vicinity of the nanoheater.

It is important to notice that in the case of nanoparticles in suspension, the distance between the nanosensors and the nanoheaters is not fixed since the sample is under stirring. Moreover, the nanoheater and ZGO-NTh are not in close contact due to the solvation sphere in the surface of each nanoparticle. Thus, the resulting measured temperature is an average of all contributions of each ZGO-NTh and we show that it does not depend on the ZGO-NTh : GNR ratio (see Fig. SI-7†). In this experiment, the obtained local nanoheater temperature is still underestimated. That is the reason why, to gain further understanding, a mixture of nanothermometers and nanoheaters has been dried under air for closer contact. The same experiment is then reproduced on a powdered sample. In this new kind of sample, distances between nanoheaters and nanothermometers are fixed and controlled for an absolute measurement. The lifetime variation according to the 976 nm laser diode excitation time is presented in Fig. 3. It appears that in contrast to measurement in aqueous suspension, the temperature variation is steep: the measured temperature reaches a maximum only a few seconds after the start of the laser excitation (red dots). However, the average temperature is about 108 ± 3 °C, which corresponds to a temperature difference of 73 ± 3 °C, in comparison with the sample composed only of nanothermometers, *i.e.* without the nanoheaters, under the same irradiation conditions (black dots). One should also notice that the temperature variation determined using the thermal camera during excitation of powder samples is very low, *i.e.* only an increase of 2 °C is observed in each case. This result is mostly due to the difference between the thermal conductivity values in water (0.6 W m^{-1} K^{-1}) and in air (0.02 W m^{-1} K^{-1}).[32]

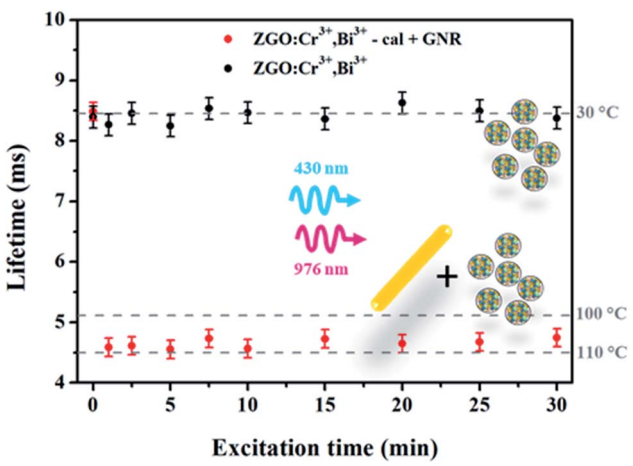

Fig. 3 Variation of the luminescence lifetime of ZGO-NTh (black) and ZGO-NTh + GNR (red) according to the laser diode excitation time.

Indeed, the thermal conductivity is a key parameter during the heat diffusion.[33] In the case of a sample in powder form, the heat is localized in the close surroundings of the particle, since air is a poor thermal conductor. Thus, the low resolution of the NIR thermal camera does not allow the detection of temperature variation at the nanoscale, in contrast to the local temperature determination through the luminescent ZGO-NTh lifetime measurements. In a dried sample, the particles are agglomerated. Due to the low air thermal conductivity, no thermalization phenomenon occurs and the temperature measurement is performed from the nanothermometer in close contact with the nanoheater. This consideration explains the difference between the temperature values extracted from the lifetime measurements for particles in water (60 ± 3 °C) or on powder (108 ± 3 °C).

Finally, to get more information about the temperature gradient around the surface GNR, the same experiment is performed with silica of several layer thicknesses around the ZGO nanoparticles to control the average distance between the nanoheater and nanothermometer. More precisely, cases are studied: ZGO-NTh after silica layer removal in alkaline medium and ZGO-NTh with, respectively, 3 nm, 5 nm and 10 nm silica layer thickness. TEM pictures of zinc gallate nanoparticles embedded in silica of several layer thicknesses are presented in Fig. 4.

Each kind of ZGO nanoparticle is then mixed with GNRs in solution with the same nanothermometer/nanoheater ratio (namely 10 : 1) before flocculation and heating to optimize the largest contact surface between the two types of nanoparticle. The luminescence lifetimes of the four powdered samples are then measured *versus* 970 nm laser diode excitation as presented in Fig. 5. The maximal value of temperature is once again reached after a few seconds. Then the luminescence lifetimes are registered alternatively after switching on and off the laser diode. The results are reported in Fig. 5, and demonstrate the reproducibility of the method, showing the robustness of the ZGO-NTh for local and absolute temperature measurements. Interestingly, the measured temperature is significantly higher when the silica shell thickness decreases and further vanishes. According to these results, it is possible to bring out the temperature gradient around the particle. More precisely, at a controlled distance of 10 nm from the gold nanorod nanoheaters, the average temperature decreases by around 70 °C in comparison to the average temperature measured at the

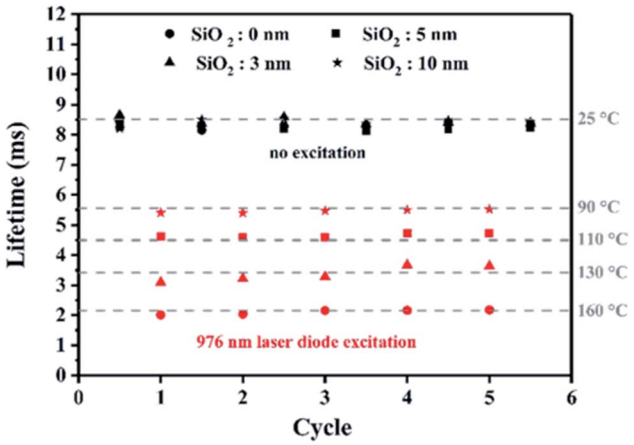

Fig. 5 Lifetime variation of ZGO-NThs embedded with silica of several layer thicknesses (0, 3, 5 and 10 nm, respectively) in the vicinity of GNRs alternatively irradiated with a 976 nm laser diode.

nanoparticle surface. Furthermore, the values of gold and silica thermal conductivities are 317 W m^{-1} K^{-1} and 1.2 W m^{-1} K^{-1}, respectively. This very important temperature variation is in good agreement with theoretical modelling reported by Ekici *et al.*[13] and Baffou *et al.*[15] Moreover, it is important to notice that the luminescent ZGO-NTh allows real time measurement in the order of a few milliseconds. At this timescale, the temperature is fully thermalized inside the particle and the only detectable gradient is around the nanoheater.

Due to the distance decrease between ZGO-NThs and nanoheaters in this configuration compared to the previous experiments in solution, it is relevant to discuss the influence of plasmon phenomenon on ZGO-NTh luminescence lifetimes that can occur at such short distance. The experimental decay which is the inverse of the lifetime can be expressed as the sum of radiative ($\Gamma_R = 1/\tau_R$) and non-radiative ($\Gamma_{NR} = 1/\tau_{NR}$) decay (see eqn (3)). The radiative part corresponds to transitions $^2E \rightarrow {}^4A_2$ and $^4T_2 \rightarrow {}^4A_2$ from levels in thermal equilibrium (SI-3†) and is associated with $\Gamma_R = 1/\tau_{fit}(T)$ (eqn (2)). The non-radiative part combines several channels. The first one corresponds to all quenching phenomena intrinsic to the ZGO-NTh (Γ_{Int}) as energy transfer channels between Cr^{3+} ions or lattice electrons/phonons for example. We also assume that luminescence processes can also be modified when emitters are close (a few nanometers) to metallic surfaces. Indeed, a coupling with

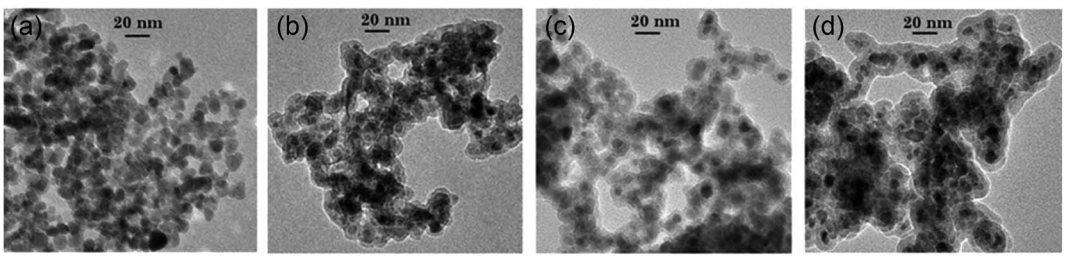

Fig. 4 TEM pictures of $ZnGa_2O_4:Cr^{3+},Bi^{3+}$ nanoparticles (a) after silica layer removal, (b) with a 3 nm silica layer, (c) with a 5 nm silica layer and (d) with a 10 nm silica layer.

surface plasmon modes can lead to an increase of non-radiative decay channels expressed by the term $\Gamma_{plasmon}$ (eqn (4)).[34,35]

$$\Gamma_{exp} = \Gamma_R + \Gamma_{NR} \quad (3)$$

$$\Gamma_{NR} = \Gamma_{Int} + \Gamma_{plasmon} \quad (4)$$

According to these considerations, the experimental lifetime slope variation can not only be attributed to the temperature increase but also to the presence of a new non-radiative channel induced by the plasmon effect. Nevertheless, as no significant change in the luminescence decay profile or in the emission spectra is observed compared to the reference sample in the presence of unexcited plasmonic nanorods (Fig. 2c and SI-8†), the role of $\Gamma_{plasmon}$ in the lifetime variation appears to be insignificant as expected because the emission wavelength is far enough from plasmon resonance. Furthermore, no clear break in the lifetime profile has been highlighted according to the silica shell thickness neither on powder samples nor in samples dispersed in water (see Fig. 6 and SI-7†), corroborating that (i) the probability of the plasmon deexcitation channel is negligible compared to the one induced by temperature ($\Gamma_{plasmon} \ll \Gamma_{Boltzmann}$) and (ii) the luminescent lifetime variation is broadly due to the temperature change.

Finally, at room temperature, no change in the luminescence lifetime profiles or in the emission spectra has been observed according to the silica layer thickness or the surrounding media (air or water, see SI-6 and SI-8†). These results demonstrate that Cr^{3+} ions at the origin of the luminescence processes are located inside the particle. Indeed, it has already been demonstrated that Cr^{3+} ions are very sensitive to their environment.[36] Due to the absence of changes in the luminescence signal according to the dielectric surrounding medium (air, water or silica), one can assume that the luminescence of ZGO-NTh results from Cr^{3+} ions far from the particle surface. Such properties make ZGO-NTh especially relevant for thermal sensor applications compared to QDs or organic dyes for which the luminescence dependence on the surrounding dielectric media has already been demonstrated.[37,38]

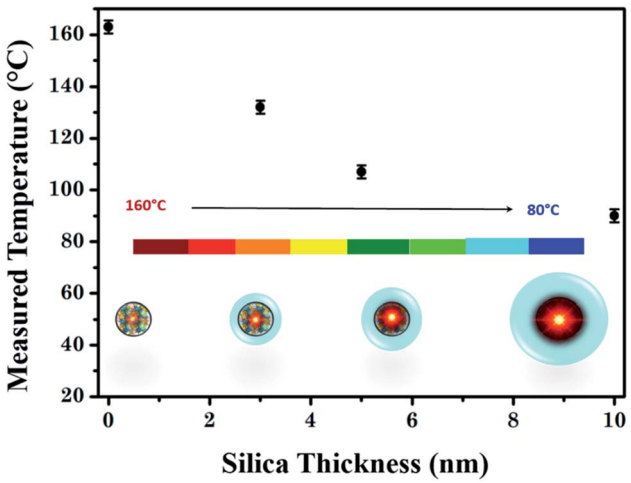

Fig. 6 Measured temperatures in the GNR surroundings as a function of silica thickness of the ZGO-NTh.

Conclusion

We demonstrated in this work the ability of luminescent chromium doped-zinc gallate oxide (ZGO) nanoparticles as thermal nanosensors. A local temperature increase after irradiation of gold nanorods (GNRs) in their plasmon resonance band has been highlighted in comparison with global thermal measurement using an NIR thermal camera. By careful control of the distance between the nanoheaters and nanothermometers, with tunable silica shell thickness, we were able to determine the temperature gradient around the nanoparticles. The strong decrease of the measured average temperature at the vicinity of the nanoheater is in good agreement with the calculated temperature profiles from the literature. We also evidence the importance of the surrounding media with different thermal conductivity values in the heat dissipation. Thus, the system composed of the coupled ZGO-NTh/GNR demonstrates the proof of concept of nanothermometry in a large temperature range and should be very promising in various application fields. This nanothermometry approach is currently undergoing considerable development because of these advantages, and this suggests routine measurements in the short term.

Methods

Materials synthesis

$ZnGa_2O_4:Cr^{3+}_{0.5\%at},Bi^{3+}_{0.5\%at}$ nanoparticles are synthesized by a hydrothermal method assisted by microwave heating. $ZnCl_2$ (≥98%), $GaCl_3$ (≥99.999%), $CrCl_3 \cdot 6H_2O$ (≥98%) and $Bi(NO_3)_3 \cdot 5H_2O$ (≥99 999%) starting materials were purchased from Sigma Aldrich. Zinc, gallium, chromium and bismuth chloride salt aqueous solutions are mixed in stoichiometric proportions. The pH of the resulting solution is adjusted to 8 by dropwise adding NaOH (4 M) solution to get an optimal hydroxylation of cations. The resulting precipitated solution is then transferred for crystallization in a microwave Teflon-lined reactor (Anton Paar, micro-wave Synthos 3000) for 1 hour heat treatment under microwave irradiation at 200 °C under continuous stirring. The obtained solid compound is then washed several times with water and dried under air. The ZGO nanoparticles are then embedded in a silica layer using a sol–gel chemistry route, to avoid sintering during the following thermal treatment. A mixture of TEOS : EtOH 1 : 5 (5 mL) is dropwise added to an ammonia solution (10 mL water + 180 μL 28% NH_3) of nanoparticles ($C = 5.3$ mg mL^{-1}). After stirring overnight, the solution is washed several times with water and dried under air. ZGO nanoparticles embedded with a 5 nm SiO_2 shell are obtained. The obtained $ZnGa_2O_4:Cr^{3+},Bi^{3+}@SiO_2$ nanoparticles are then calcined in air for 2 h at 1000 °C using a 10 °C per minute ramp to improve the quantum efficiency of chromium emitters. The thickness of the silica layer can be controlled by the quantity of ammonia and TEOS introduced in the starting solution. For a 3 nm SiO_2 shell 120 μL of NH_3 solution is added, which slows the condensation process of silica. An important increase of

ammonia or TEOS can lead to SiO_2 nanoparticle synthesis (homogeneous nucleation). That is why, for ZGO nanoparticles embedded with 10 nm SiO_2, a three times repeat of the process presented below is preferred. The silica layer is removed using a basic treatment (NaOH 2 M, one-night stirring, $C_{ZGO} = 2.5$ mg mL^{-1}). All ZGO samples are dispersed in water at pH = 5.

Gold nanorods are synthesized using a binary surfactant method adapted from Murray *et al.*[39] A seeded solution is first prepared by mixing the gold precursor ($HAuCl_4$, $n = 2.5 \times 10^{-6}$ mol) and surfactant (CTAB, $n = 1.0 \times 10^{-3}$ mol); a freshly prepared $NaBH_4$ solution ($n = 6.0 \times 10^{-6}$ mol) is then added to the previous solution as a reducing agent. After stirring, the color of the solution changed from yellow to brown. This seeded solution is then added to the growth solution prepared as follows: $AgNO_3$ solution is added to a surfactant mixture of CTAB and oleic acid ($n = 1.9 \times 10^{-2}$ mol and 4.0×10^{-3} mol, respectively); after 15 min without stirring, $HAuCl_4$ is added ($n = 2.5 \times 10^{-4}$ mol) and the solution becomes colorless after about 90 min of stirring. HCl is then added to adjust the pH value. Finally, after another 15 min stirring, ascorbic acid ($n = 8.0 \times 10^{-5}$ mol) is added to the mixture. The final solution is then washed several times after being left for 12 h undisturbed. At the end, an aqueous suspension of gold nanoparticles is obtained which is stable at pH = 5.

In order to couple nanoheaters to nanothermometers, the GNRs and ZGO-NThs are simply mixed in solution with a ZGO : GNR ratio of 10 : 1. The ZGO suspension is added to the gold suspension. A heteroaggregation of both particle types occurs as observed by TEM on the frozen droplet of the suspension (Fig. SI-5†) suggesting a strong interaction between the two types of particle. As a result, the suspension is destabilized and then optical spectra are recorded under continuous stirring. This coupled system is also dried under air to perform measurements on powder.

Structural and optical characterization

X-ray diffraction patterns are obtained by powder X-ray diffraction (PW-XRD) using a Bruker D8 Advance diffractometer with Cu-Kα radiation ($\lambda = 1.5406$ Å) at 30 kV and 40 mA, 0.0017° 2θ step size and 1 s step time over 2θ of 10 to 70°. Transmission electron microscopy (TEM) pictures are taken using a Technai G2 Spirit apparatus, and the images are recorded on a CCD camera (Orius Gatan 832 digital). Carbon coated with copper TEM grids are used, after evaporation of one drop of aqueous nanoparticle suspension. Absorption spectra of gold nanoparticles are registered with a UV-visible NIR spectrometer, CARY 5000 – Agilent Technologies. Excitation and emission spectra of ZGO nanoparticles are registered with a Cary Eclipse Varian spectrophotometer in phosphorescence mode. Photoluminescence decay spectra are obtained after excitation provided by an Optical Parametric Oscillator (OPO) YAG:Nd pulsed laser (EKSPLA 342B) and recorded *via* a photomultiplier coupled to an oscilloscope. A LIMO-7 continuous laser diode ($\lambda = 976$ nm) coupled to an optical fiber is used for GNR excitation ($P = 3$ W cm^{-2}). Thermal pictures are taken with a FLIR E4 camera.

Conflicts of interest

No conflicts of interest have been declared.

Acknowledgements

This work was supported by the Cluster of Excellence MATISSE, by DGA (Direction Générale de l'Armement, France), and by the European Union's Horizon 2020 FET Open program (project NanoTBTech, grant number 801305).

References

1 A. A. Wahab, *et al.*, Thermal distribution analysis of three-dimensional tumor-embedded breast models with different breast density compositions, *Med. Biol. Eng. Comput.*, 2016, **54**, 1363–1373.
2 D. Singh and A. K. Singh, Role of image thermography in early breast cancer detection-past, present and future, *Comput. Meth. Prog. Bio.*, 2020, **183**, 105074.
3 C. S. S. R. Kumar and F. Mohammad, Magnetic nanomaterials for hyperthermia-based therapy and controlled drug delivery, *Adv. Drug Delivery Rev.*, 2011, **63**, 789–808.
4 J. M. Asensio, A. B. Miguel, P.-F. Fazzini, P. W. N. M. van Leeuwen and B. Chaudret, Hydrodeoxygenation Using Magnetic Induction: High-Temperature Heterogeneous Catalysis in Solution, *Angew. Chem.*, 2019, **131**, 11428–11432.
5 L. Gao, *et al.*, Single-cell photoacoustic thermometry, *J. Biomed. Opt.*, 2013, **18**, 026003.
6 J. Zhou, B. del Rosal, D. Jaque, S. Uchiyama and D. Jin, Advances and challenges for fluorescence nanothermometry, *Nat. Methods*, 2020, **17**, 967–980.
7 F. Vetrone, *et al.*, Temperature Sensing Using Fluorescent Nanothermometers, *ACS Nano*, 2010, **4**, 3254–3258.
8 C. D. S. Brites, *et al.*, Thermometry at the nanoscale, *Nanoscale*, 2012, **4**, 4799.
9 D. Jaque and F. Vetrone, Luminescence nanothermometry, *Nanoscale*, 2012, **4**, 4301.
10 E. J. McLaurin, L. R. Bradshaw and D. R. Gamelin, Dual-Emitting Nanoscale Temperature Sensors, *Chem. Mater.*, 2013, **25**, 1283–1292.
11 L. D. Carlos and F. Palacio, *Thermometry at the Nanoscale: Techniques and Selected Applications*, Royal Society of Chemistry, 2015.
12 A. O. Govorov, *et al.*, Gold nanoparticle ensembles as heaters and actuators: melting and collective plasmon resonances, *Nanoscale Res. Lett.*, 2006, **1**, 84–90.
13 O. Ekici, *et al.*, Thermal analysis of gold nanorods heated with femtosecond laser pulses, *J. Phys. D: Appl. Phys.*, 2008, **41**, 185501.
14 A. O. Govorov and H. H. Richardson, Generating heat with metal nanoparticles, *Nano Today*, 2007, **2**, 30–38.
15 G. Baffou and R. Quidant, Thermo-plasmonics: using metallic nanostructures as nano-sources of heat: thermoplasmonics, *Laser Photonics Rev.*, 2013, **7**, 171–187.

16 A. Carattino, M. Caldarola and M. Orrit, Gold Nanoparticles as Absolute Nanothermometers, *Nano Lett.*, 2018, **18**, 874–880.
17 U. Rocha, *et al.*, Subtissue Thermal Sensing Based on Neodymium-Doped LaF_3 Nanoparticles, *ACS Nano*, 2013, **7**, 1188–1199.
18 L. M. Maestro, *et al.*, Fluorescent nanothermometers provide controlled plasmonic-mediated intracellular hyperthermia, *Nanomedicine*, 2013, **8**, 379–388.
19 M. L. Debasu, *et al.*, All-In-One Optical Heater-Thermometer Nanoplatform Operative From 300 to 2000 K Based on Er^{3+} Emission and Blackbody Radiation, *Adv. Mater.*, 2013, **25**, 4868–4874.
20 L. M. Maestro, Q. Zhang, X. Li, D. Jaque and M. Gu, Quantum-dot based nanothermometry in optical plasmonic recording media, *Appl. Phys. Lett.*, 2014, **105**, 181110.
21 L. M. Maestro, *et al.*, Quantum Dot Thermometry Evaluation of Geometry Dependent Heating Efficiency in Gold Nanoparticles, *Langmuir*, 2014, **30**, 1650–1658.
22 K. Nigoghossian, *et al.*, Upconversion nanoparticle-decorated gold nanoshells for near-infrared induced heating and thermometry, *J. Mater. Chem. B*, 2017, **5**, 7109–7117.
23 Y. Huang, *et al.*, Upconverting nanocomposites with combined photothermal and photodynamic effects, *Nanoscale*, 2018, **10**, 791–799.
24 E. Glais, *et al.*, Luminescence properties of $ZnGa_2O_4:Cr^{3+},Bi^{3+}$ nanophosphors for thermometry applications, *RSC Adv.*, 2018, **8**, 41767–41774.
25 W. Mikenda and A. Preisinger, N-lines in the luminescence spectra of Cr^{3+}-doped spinels (I) identification of N-lines, *J. Lumin.*, 1981, **26**, 53–66.
26 W. Mikenda and A. Preisinger, N-lines in the luminescence spectra of Cr^{3+}-doped spinels (II) origins of N-lines, *J. Lumin.*, 1981, **26**, 67–83.
27 J. Ueda, *et al.*, Ratiometric optical thermometry using deep red luminescence from $^4T_2$ and ^2E states of Cr^{3+} in $ZnGa_2O_4$ host, *Opt. Mater.*, 2018, **85**, 510–516.
28 D. Chen, Z. Wan and Y. Zhou, Optical spectroscopy of Cr^{3+}-doped transparent nano-glass ceramics for lifetime-based temperature sensing, *Opt. Lett.*, 2015, **40**, 3607.
29 O. Labeau, P. Tamarat and B. Lounis, Temperature Dependence of the Luminescence Lifetime of Single CdSe/ZnS Quantum Dots, *Phys. Rev. Lett.*, 2003, **90**, 257404.
30 M. G. Brik, N. M. Avram and C. N. Avram, Comparative crystal field calculations of the Cr^{3+} energy level schemes in $ZnAl_2S_4$ and $ZnGa_2O_4$, *J. Mater. Sci.: Mater. Electron.*, 2009, **20**, 30–32.
31 E. Glais, V. Đorđević, J. Papan, B. Viana and M. D. Dramićanin, $MgTiO_3:Mn^{4+}$ a multi-reading temperature nanoprobe, *RSC Adv.*, 2018, **8**, 18341–18346.
32 B. L. Neindre, *Conductivité thermique des liquides et des gaz. Ref: TIP510WEB – 'Constantes physico-chimiques'*, https://www.techniques-ingenieur.fr/base-documentaire/42340210-equations-d-etats-et-constantes-thermiques/download/k427/conductivite-thermique-des-liquides-et-des-gaz.html, 1998.
33 T. L. Bergman, F. P. Incropera, A. S. Lavine and D. P. DeWitt, *Introduction to Heat Transfer*, John Wiley & Sons, 2011.
34 E. Fort and S. Grésillon, Surface enhanced fluorescence, *J. Phys. D: Appl. Phys.*, 2008, **41**, 013001.
35 C. Vion, *et al.*, Controlled modification of single colloidal CdSe/ZnS nanocrystal fluorescence through interactions with a gold surface, *Opt. Express*, 2010, **18**, 7440.
36 D. Gourier, *et al.*, Origin of the visible light induced persistent luminescence of Cr^{3+}-doped zinc gallate, *J. Phys. Chem. Solids*, 2014, **75**, 826–837.
37 Y. Zhao, *et al.*, High-Temperature Luminescence Quenching of Colloidal Quantum Dots, *ACS Nano*, 2012, **6**, 9058–9067.
38 G. Lamouche, P. Lavallard and T. Gacoin, Optical properties of dye molecules as a function of the surrounding dielectric medium, *Phys. Rev. A: At., Mol., Opt. Phys.*, 1999, **59**, 4668–4674.
39 X. Ye, C. Zheng, J. Chen, Y. Gao and C. B. Murray, Using Binary Surfactant Mixtures To Simultaneously Improve the Dimensional Tunability and Monodispersity in the Seeded Growth of Gold Nanorods, *Nano Lett.*, 2013, **13**, 765–771.